COMMUNICATION

ADVANCED
MATERIALS
www.advmat.d

Check for
updates

Wavelength-Tunable Mid-Infrared Lasing from Black Phosphorus Nanosheets

Yushuang Zhang, Shaowei Wang, Shula Chen, Qinglin Zhang, Xiao Wang, Xiaoli Zhu, Xuehong Zhang, Xing Xu, Tiefeng Yang, Mai He, Xin Yang, Ziwei Li, Xu Chen, Mingfei Wu, Yuerui Lu, Renmin Ma, Wei Lu,* and Anlian Pan*

Van der Waals layered semiconductor materials own unique physical properties and have attracted intense interest in developing high-performance electronic and photonic devices. Among them, black phosphorus (BP) is distinct for its layer number-tuned direct band gap which spans from near- to mid-infrared (MIR) waveband. In addition, the puckered honey comb crystal lattice endows the material with highly linear-polarized emission and marked anisotropy in carrier transportation. These unique material properties render BP as an intriguing and promising building block for constructing mid-infrared-ranged coherent light sources. Here, a room temperature surface-emitting MIR laser based on single crystalline BP nanosheets coupled with a distributed Bragg reflector cavity is reported. MIR stimulated emission at 3611 nm is achieved with a near-unity linear polarization, which exhibits robust thermal stability up to 360 K. Most importantly, the lasing wavelength can be tuned from 3425 to 4068 nm by varying the cavity length via thickness control of BP layer. The demonstrated highly polarized lasing output and wavelength-tunable capacity of the proposed device scheme in MIR spectral range opens up promising opportunities for a broad array of applications in polarization-resolved IR imaging, range-finding, and free space quantum communications.

Van der Waals layered semiconductor materials have shown great potentials in the future high-performance electronic, photonic, and optoelectronic devices, due to their unique physical properties.[1–3] Lasing investigation in thin layered materials have aroused great interest recently, due to their

potential applications in integrated photonics for on-chip optical interconnects, gas sensing, and imaging applications.[4–6] Thus far, almost all the reported works are limited to the visible region to near-infrared (near-IR) waveband. Pushing the laser wavelength of van der Waals crystal-based nano-emitters further into IR spectral range is of paramount significance for sensing and free space telecommunication technologies. In light of the intriguing prospect, black phosphorus (BP), in recent years, has emerged as a promising material for IR-oriented nanophotonic applications. This is driven by the facts that BP possesses a layer-dependent direct bandgap character, greatly different from other 2D transition metal dichalcogenide materials.[7,8] By increasing the thickness of BP from monolayer to bulk, the band gap of BP decreases from ≈1.75 eV to ≈0.3 eV, spanning almost all the near- to mid-IR (MIR) spectral region.[8] More importantly, the unique crystalline structure of BP enables strong in-plane anisotropy of both electrical and optical properties, which can be harnessed for novel physical effects.[9–12] The high carrier mobility has already demonstrated BP's superiority in a wealth of nanoelectronics devices.[13–17] All these merits render BP an ideal building block for potential applications in integrated electronics and

Y. S. Zhang, Prof. S. L. Chen, X. Yang, Prof. Z. W. Li, Prof. A. L. Pan
Key Laboratory for Micro-Nano Physics and Technology of Hunan Province
State Key Laboratory of Chemo/Biosensing and Chemometrics
College of Materials Science and Engineering
Hunan University
Changsha, Hunan 410082, China
E-mail: anlian.pan@hnu.edu.cn
Prof. S. W. Wang, X. Chen, M. F. Wu, Prof. W. Lu
State Key Laboratory of Infrared Physics
Shanghai Institute of Technical Physic
Chinese Academy of Sciences
Shanghai 200083, China
E-mail: luwei@mail.sitp.ac.cn

The ORCID identification number(s) for the author(s) of this article can be found under https://doi.org/10.1002/adma.201808319.

Prof. Q. L. Zhang, Prof. X. Wang, Prof. X. L. Zhu, X. H. Zhang, X. Xu, T. F. Yang, M. He
Key Laboratory for Micro-Nano Physics and Technology of Hunan Province
School of Physics and Electronic Science
Hunan University
Changsha, Hunan 410082, China
Prof. Y. R. Lu
Research School of Engineering
College of Engineering and Computer Science
Australian National University
Canberra, ACT 2601, Australia
Prof. R. M. Ma
State Key Lab for Mesoscopic Physics and School of Physics
Peking University
Beijing 100871, China

optoelectronics operated at IR spectral range. To date, majority of optical studies on BP have been related to spontaneous emission (SPE) from few-layer structures with the spectral response in the near-IR to MIR spectral region.[18–20] Most recently, MIR lasing from lamellar BP thin film layers with random nanogaps was reported, which is configured in an open distributed Bragg reflector (DBR) cavity device structure,[21] However, more solid results are needed to clarify the evolution from amplified SPE to lasing. To be mature for laser application, high crystalline quality of gain medium, temperature robustness, and wavelength tunability of the device usually lie at the heart of their opto-electronic performance. In this work, we report a temperature-robust and wavelength-tunable MIR lasers from single crystalline BP nanosheets of premium quality, which is coupled with high quality DBR cavity. Sharp lasing radiation at 3600 nm was achieved with an emission line narrowing down to ≈7 nm. The lasing emission shows pronounced liner polarization along the armchair axis as determined by crystalline anisotropy of the BP. By varying the cavity length via controlling BP nanosheet thickness, the stimulated emission wavelength can be facilely tuned from 3425 to 4068 nm, without invoking alloy engineering as commonly adopted by other conventional semiconductor materials. Furthermore, the proposed BP-based MIR laser can operate up to 360 K, exhibiting high temperature stability for device application. Endowed with prominent material properties and device performance, thin layered BP holds great potential as highly linear-polarized coherent photon source for opto-electronic applications in MIR range.

The proposed device structure of thin layered BP laser is schematically shown in **Figure 1**a, where a SiO cavity (containing a thin single crystalline BP layer embedded in the cavity) is sandwiched between a bottom and a top DBR (detailed fabrication method see Section S1, Supporting Information). The model analysis shows the optical confinement factor of the active region (BP nanosheet with 100 nm thickness) in the DBR microcavity was simulated to be ≈2.0% (see Figure S1, Supporting Information). Figure 1b gives the cross-section scanning electron microscope (SEM) image of the DBR cavity, which is composed of well-defined periodic silicon monoxide/silicon (SiO/Si) films for both the bottom (five pairs) and the top (six pairs) of the structure, with a piece of BP thinlayer, marked by arrow, embedded in two SiO spacers in the cavity. The transmission spectrum of the bottom DBR on silicon substrate shows a reflection band from 3.35 to 4.61 μm with the reflectivity of ≈99% (see Figure 1d), which is well matched to the light emission of BP at the MIR region. After transferring a sheet of BP onto the bottom DBR and covering it with another top DBR, the obtained device exhibits two narrow passbands centered at the wavelength of ≈4494 nm (0.276 eV) and ≈3700 nm (0.335 eV), respectively, corresponding to the third and the fourth order of the resonance mode in cavity. We observed a full width at half maximum (FWHM) of 12.6 nm (10.5 nm) for the third (fourth) order of modes (see Figure 1d and Figure S2, Supporting Information), which indicates a quality (Q)-factor of ≈350.

The optical performance of gain medium is at the heart of a laser device. We first examined MIR-ranged photoluminescence (PL) emission of single crystalline BP thinlayers outside the DBR cavity using home-made IR micro-PL detection system (see Figure S3, Supporting Information). **Figure 2**a
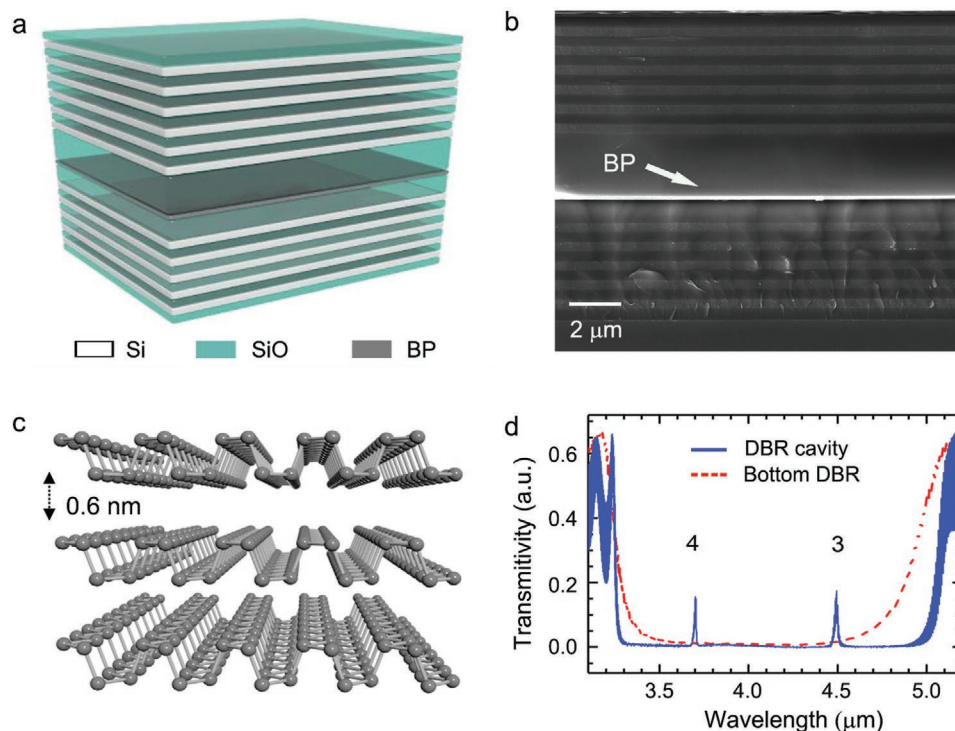

Figure 1. a) Schematic diagram of BP nanosheets imbedded in the DBR microcavity. b) The SEM image of BP embedded in the DBR microcavity for the cross-section view. Scale bar denotes 2 μm. c) The schematic of crystalline structure of BP layer. d) The transmission spectrum of bottom DBR (dashed line) and the SiO cavity sandwiched between the bottom and up DBRs (solid line), respectively.
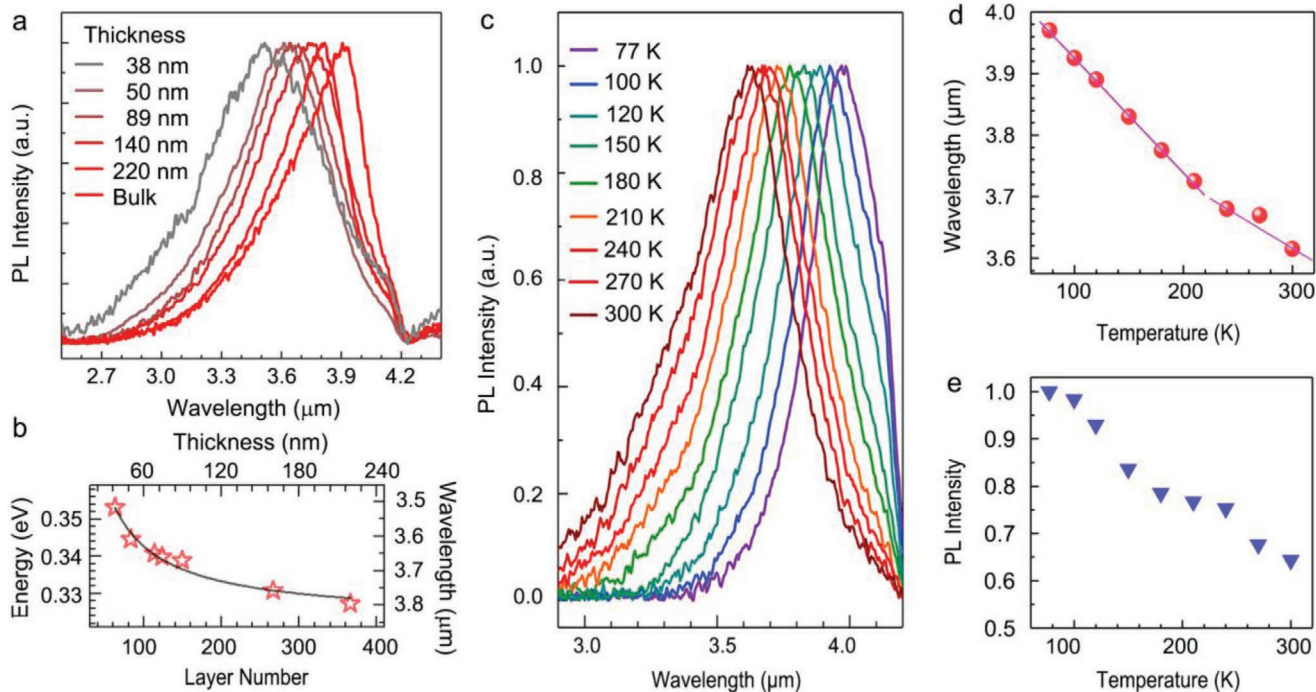
Figure 2. a) The PL emission spectra of BP nanosheets with different thickness. b) The layer dependent PL peak energy. Stars and solid line are the experiment data and the fitted result, respectively. c) The PL spectra of one representative BP nanosheet at different temperature. d) The temperature-dependent peak wavelength plot. e) The temperature dependent emission intensity plot. The dips at 4.23 μm in (a) and (c) are attributed to the absorption of CO_2 in the air.

gives the room-temperature PL spectra of BP bulk and thin layers with the thickness of 38, 50, 89, 140, and 220 nm, respectively. Strong MIR emissions can be detected from all these samples, with a gradual shift of the peak wavelength from 3505 to 3920 nm when the thickness is increased from 38 nm to the bulk size. The layer number-dependent PL peak energy can be extracted from Figure 2a through dividing the thickness by monolayer thickness of BP, 0.6 nm, which can be fitted by the power law relation and is in good agreement with the theoretical prediction of layer thickness-dependent band gap of BP, (see Figure 2b and Section S6, Supporting information).[7,8,11] These results demonstrate BP as excellent room-temperature optical-gain material in the MIR region.

Temperature plays an important role on changing semiconductors band gap and also emission intensity due to thermally activated nonradiative recombination process, which can closely affect the operation threshold of device. Therefore, temperature-dependent measurement was performed to investigate the optical performance of BP as the gain medium for MIR lasing at room temperature. Figure 2c is the temperature dependent PL spectra of the BP thinlayer with a thickness of ≈60 nm, which shows an unambiguous red-shift of the peak wavelength from 3620 to 3970 nm when the temperature is decreased from 300 to 77 K (see Figure 2d). This red-shift phenomenon is consistent with the observation on few layer BP and is also in agreement with the recent theory prediction on bulk BP, which is attributed to both the electron–phonon coupling and the lattice thermal expansion.[22,23] The temperature dependent peak energy can be fitted by two linear functions (see the solid lines in Figure 1d), with the slopes of 0.111 and 0.156 meV K^{-1} for the

temperature ranging from 300 to 210 K and from 210 to 77 K, respectively, which accords well with previous theoretical prediction and photoconduction measurements.[23,24] Generally, an increasing temperature leads to a decreased PL emission intensity, due to thermal activation of the nonradiative recombination centers and/or dissociation of the excitons.[22,25] From the temperature dependent PL measurement shown in Figure 2e, an activation energy of 24.7 ± 4.9 meV can be obtained by fitting with the Arrhenius formula (see Figure S4, Supporting Information).[25] This value is lower than the reported exciton binding energy of bulk BP.[8] The result indicates that the decreased PL intensity at higher temperature is caused by the thermal occupation of nonradiative recombination centers rather than the excitons dissociation. The small decrease in PL intensity with rising temperature suggests the density of the nonradiative recombination center is limited in the BP nanosheets, which contributes to the observed strong room-temperature PL emission even at room temperature. The above discussions prove that the single crystalline BP thinlayers are ideal MIR excitonic gain media at room temperature.

Next, with the assistance of high quality DBR microcavity, we demonstrated the optically pumped MIR lasing from these excellent MIR gain media based on the single crystalline BP thinlayers at room temperature. The excitation power dependent emission spectra of a BP thinlayer (100 nm thick) embedded in the DBR cavity pumped at high and low power with a femtosecond laser of 1520 nm (pulse duration: 80 fs, repetition rate: 1KHz) and a Nd:YAG laser at the wavelength of 1064 nm (pulse duration: 150 ns, repetition rate: 50 KHz) are given in **Figure 3**a,b, respectively. A broad emission band centered at 3640 nm with
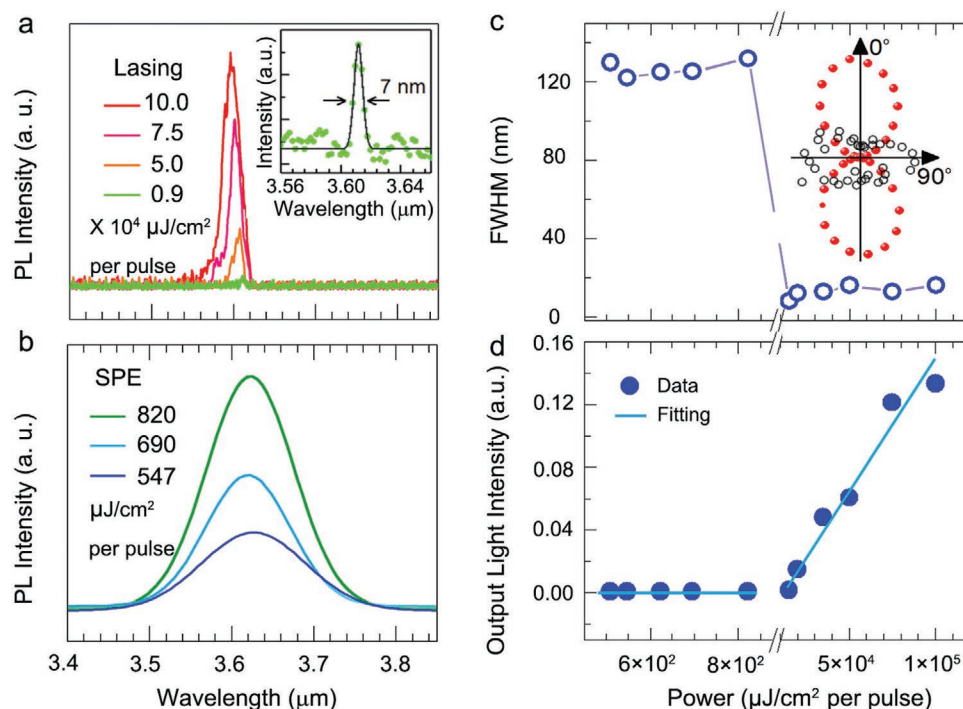
Figure 3. a) The pumping power dependent emission spectra of BP embedded in the DBR microcavity in lasing radiation. Inset shows the spectrum measured at the peak power of 15 mJ cm^{-2} per pulse. The solid line in the inset is the fitted result by Gaussian function. b) Pumping power dependent emission spectra in spontaneous emission regime. c) FWHM as a function of pumping fluence, the PL polarization of lasing and SPE are shown as solid and open dots in inset. d) The pumping power dependent emission intensity of the device.

the FWHM of ≈171 nm is observed, and the emission intensity increases linearly with the increase of the pumping power from 547 to 883 µJ cm^{-2} per pulse, coming from the SPE of the BP nanosheet in the cavity. Further examination indicates that the emission intensity will decrease when the power is above 750 µJ cm^{-2} per pulse (see Figure S5, Supporting Information), and the structures will be destroyed under a too high power pumping, induced by the thermal effect of the long pulse duration laser. To minimize this thermal effect at high power and obtain enough gain to realize optical amplification, a femtosecond laser of 1520 nm was used to pump the device at higher power levels. As shown in Figure 3a, the device outputs a sharp emission line at the wavelength of 3611 nm with the FWHM of only ≈7 nm (see the inset) when it was pumped at the peak power of 9 mJ cm^{-2} per pulse, without any obvious broad SPE background. The corresponding Q-factor of the emission line is 516, higher than that of the passive cavity mode (300), which indicates the high gain-cavity coupling between the BP nanosheet and the DBR cavity mode.[26] This significant narrowing of FWHM relative to both the SPE and the passive cavity mode indicates the occurrence of lasing (see the power dependent FWHM in Figure 3c).[26,27] The lasing wavelength at 3611 nm (rather than at the wavelength of the third or the fourth order cavity mode) corresponds to the shift of the fifth order cavity mode (3147 nm) to the longer wavelength, resulting from the increase of the cavity length by inserting the 100 nm thick BP thinlayer into the SiO cavity (see Section S9, Supporting information). When the pumping power was gradually increased to 25 mJ cm^{-2} per pulse, the emission intensity shows a fast increase, with the lineshape and the peak position almost unchanged. As the pumping power reached 50 mJ cm^{-2}

per pulse, the FWHM of emission line was quickly broadened to 25 nm with the peak wavelength slightly blue-shift to 3596 nm, which are attributed to both the heating effect and the carrier density increase.[6,28] The integrated emission intensity against pumping power was plotted in Figure 3d, where the intensity was normalized to per pulse by dividing the measured intensity with the laser repetition rate. Under the low power excitation, the integrated emission intensity shows a linear increase with the power, and it increases much more rapidly under the high pumping power regime, showing a superlinear profile of the emission output, which further proves the lasing behavior of the device.[29] The lasing threshold can be extracted from the fitting to be about 1.3 mJ cm^{-2} per pulse, corresponding to the average power of 1.3 W cm^{-2} (diameter of the pumping laser spot is 100 µm), which is comparable to the recently reported thresholds of monolayer transition metal sulfur compounds lasing at room temperature (0.44–6.6 W cm^{-2}).[6]

The polarization of the lasing is an important property of lasers. Inset of Figure 3c shows the plots of emission peak intensity as a function of polarization angle (θ) for both lasing (solid dots) and SPE (open dots), where the PL polarization for lasing and SPE are orthogonal to each other in two excitation regimes. Monolayer and few-layer BP has been proved to have strong anisotropy due to its unique puckered honeycomb structure with different behaviors along the two orthogonal direction of armchair and zigzag (see Figure 1c). According to the selection rules, the polarization direction of both the SPE and absorption are parallel to the armchair direction because its optical transition is permitted by the symmetry.[7,11] When the emission resonates in the cavity as schematically shown in **Figure 4**a, the
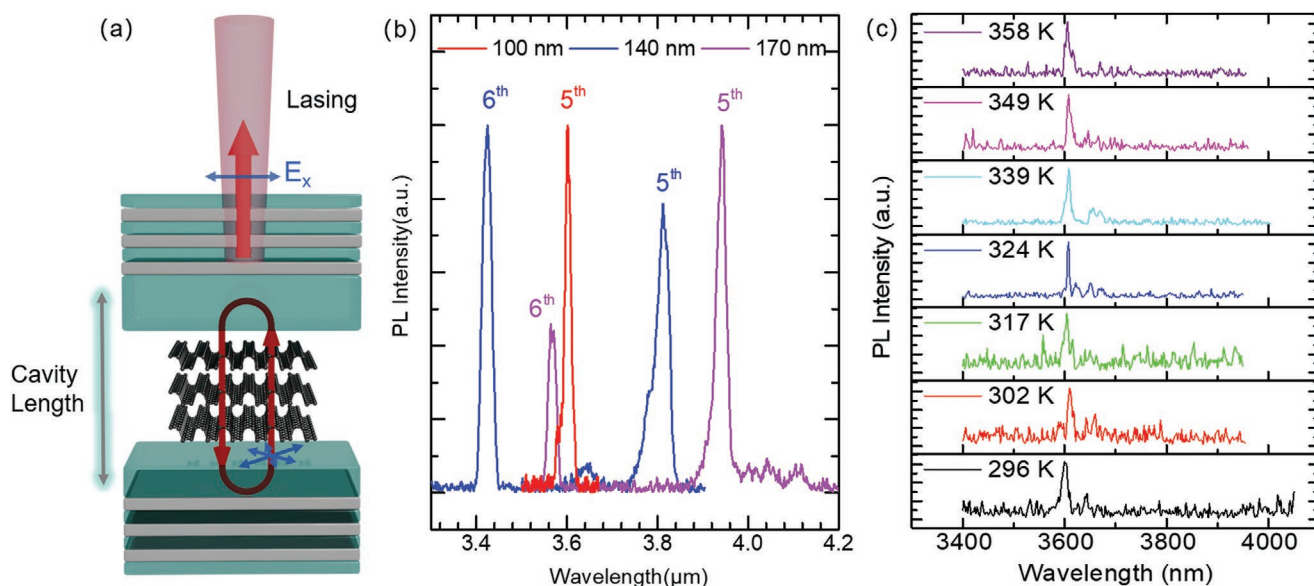
Figure 4. a) The schematic of light resonance in the DBR microcavity. The closed loop with the arrows denotes the resonance of the emission light. The orthogonal arrows denote the polarization of the light, where E_x, E_y are the electric field along the arm chair and zigzag direction of BP. The cavity length includes the thickness of BP nanosheet and the adjacent SiO layers. b) The lasing spectra of the devices with the same SiO spacer and different thickness BP (140 nm and 170 nm), pumped at 20 mJ cm^{-2} per pulse of femtosecond laser. The result measured at the same condition of the device with 100 nm BP thin layer is also presented for comparison. c) Temperature-dependent lasing spectra of 140 nm-thick BP device.

light with the polarization along the armchair direction will be re-absorbed more significantly than that along the zigzag direction, which indicates that the latter will be gained more easily than the former due to the relative lower round-trip loss. As a result, the polarization of the lasing should be along the zigzag direction perpendicular to SPE, which is consistent with the results of PL polarization measurement in inset of Figure 3c. The polarization degree, defined as $P = (I_{max} - I_{min})/(I_{max} + I_{min})$, is determined to be 97% and 48% respectively for the lasing and the SPE, which results from the selection of mode by the resonant DBR cavity and further confirms the lasing behavior at high pumping power. The high polarization degree further demonstrates the formation of coherent emission of BP in the DBR cavity at the MIR region. In addition, the lasing wavelength and mode number can be tuned by altering the thickness of BP thin layers to modify the cavity length, as described in Figure 4a and Section S9, Supporting Information. Figure 4b shows the lasing spectra of the devices with the BP thin layer thickness of about 140 nm (the blue curve) and 170 nm (the pink curve), pumped by the 10 mJ cm^{-2} per pulse femtosecond laser. Different from single-mode lasing of the device with 100 nm thick BP shown in Figure 3 (presented as red curve in Figure 4 for comparison), both devices show a double-mode lasing. Because the increase of cavity length due to the insertion of BP thin layers will cause the corresponding mode to shift to the longer wavelength with the length of about $2n_p d_p$ ($n_p = 2.4$, and d_p are the reflectivity index and thickness of BP), the lasing at 3812 nm (140 nm thick BP) and 3942 nm (170 nm thick BP) can be considered as the shift from original modes at 3140 and 3126 nm, respectively, which agrees with the fifth order mode at 3147 nm. Simultaneously, another mode at 3425 and 3563 nm are attributed to the shift from the modes respectively at 2753 and 2747 nm, corresponding to the sixth

order mode at 2735 nm. For comparison, the sixth and fourth order modes of the device with 100 nm thick BP are respectively at 3217 nm (out of the stop band, shown in Figure 1d) and 4180 nm (out of optical gain region, shown in Figure 2a), which makes only the fifth order mode observable. These results indicate that the wavelength of the lasing can be tuned from 3425 to 3942 nm, and tuned from single to dual wavelength lasing by changing the thickness of the inserted optical gain thin layer. Although the wavelength was currently tuned on different chips, the further improvements can be realized with combinatorial etching technique, or position related nanosheet thickness control techniques, by which different resonance wavelength of DBR cavities can be integrated on a single chip. Finally, the temperature robustness of a laser device is essentially important for its reliable operation and practical nanophotonic application. To evaluate the thermal stability of the BP laser, temperature-dependent PL measurement was performed by pumping the device in stimulated emission regime. The mid-IR-ranged lasing at 3600 nm was observed up to 358 K from the representative 100 nm-thick BP device. The lasing peak position exhibits negligibly small shift versus temperature, demonstrating the temperature stability of the dielectric DBR resonator and thermal robustness of the BP gain medium.

In summary, we have demonstrated MIR lasing from single crystalline BP nanosheets embedded in the dielectric DBR microcavity up to 360 K. The high operation temperature benefits from the strong excitonic emission of BP and the coupling factor of the DBR micro cavity, 1%. Based on the thickness dependent cavity mode, both the lasing wavelength and mode number can be tuned by changing the thickness of the inserted BP thin layers. The emission polarization studies show an orthogonal polarization direction and an increased polarization degree (97%) for lasing compared with that for SPE, which is

ADVANCED
SCIENCE NEWS
www.advancedsciencenews.com

ADVANCED
MATERIALS
www.advmat.de

resulted from the anisotropic round-trip loss in BP nanosheets. The present IR lasing wavelength can be continuously extended to near-IR region through decreasing the thickness of BP nanosheets. The realization of the wide wavelength tunable IR laser of BP widens the applications of 2D materials in the future silicon-based on-chip integrated photonics systems.

Supporting Information

Supporting Information is available from the Wiley Online Library or from the author.

Conflict of Interest

The authors declare no conflict of interest.

Author Contributions

Y.Z., S.W., and S.C. contributed equally to this work as first authors. A.P. and W.L. conceived and designed the experiments. S.W., X.C, M.W., and W.L. fabricated the black phosphorus laser device. Y.Z. and Q.Z. performed all PL measurements and interpret the data. A.P., Q.Z., and Y.Z. wrote the paper with significant inputs from R.M., Y.L., F.X., A.P. supervised the research work. All the authors participated in the analysis of the data and discussed the results. All the authors have read and approved the manuscript.

[1] K. F. Mak, J. Shan, *Nat. Photonics* **2016**, *10*, 216.
[2] J. R. Schaibley, H. Yu, G. Clark, P. Rivera, J. S. Ross, K. L. Seyler, W. Yao, X. Xu, *Nat. Rev. Mater.* **2016**, *1*, 16055.
[3] Y. Liu, N. O. Weiss, X. Duan, H.-C. Cheng, Y. Huang, X. Duan, *Nat. Rev. Mater.* **2016**, *1*, 16042.
[4] S. Wu, S. Buckley, J. R. Schaibley, L. Feng, J. Yan, D. G. Mandrus, F. Hatami, W. Yao, J. Vučković, A. Majumdar, X. Xu, *Nature* **2015**, *520*, 69.
[5] Y. Ye, Z. J. Wong, X. Lu, X. Ni, H. Zhu, X. Chen, Y. Wang, X. Zhang, *Nat. Photonics* **2015**, *9*, 733.
[6] Y. Li, J. Zhang, D. Huang, H. Sun, F. Fan, J. Feng, Z. Wang, C. Z. Ning, *Nat. Nanotechnol.* **2017**, *12*, 987.
[7] L. Li, J. Kim, C. Jin, G. J. Ye, D. Y. Qiu, F. H. da Jornada, Z. Shi, L. Chen, Z. Zhang, F. Yang, K. Watanabe, T. Taniguchi, W. Ren, S. G. Louie, X. H. Chen, Y. Zhang, F. Wang, *Nat. Nanotechnol.* **2017**, *12*, 21.
[8] V. Tran, R. Soklaski, Y. Liang, L. Yang, *Phys. Rev. B.* **2014**, *89*, 235319.
[9] J. Qiao, X. Kong, Z.-X. Hu, F. Yang, W. Ji, *Nat. Commun.* **2014**, *5*, 4475.
[10] F. Xia, H. Wang, Y. Jia, *Nat. Commun.* **2014**, *5*, 4458.
[11] X. Wang, A. M. Jones, K. L. Seyler, V. Tran, Y. Jia, H. Zhao, H. Wang, L. Yang, X. Xu, F. Xia, *Nat. Nanotechnol.* **2015**, *10*, 517.
[12] A. S. Rodin, A. Carvalho, A. H. C. Neto, *Phys. Rev. B* **2014**, *90*, 7.
[13] H. Liu, A. T. Neal, Z. Zhu, Z. Luo, X. Xu, D. Tománek, P. D. Ye, *ACS Nano* **2014**, *8*, 4033.
[14] L. Li, Y. Yu, G. J. Ye, Q. Ge, X. Ou, H. Wu, D. Feng, X. H. Chen, Y. Zhang, *Nat. Nanotechnol.* **2014**, *9*, 372.
[15] X. Chen, Y. Wu, Z. Wu, Y. Han, S. Xu, L. Wang, W. Ye, T. Han, Y. He, Y. Cai, N. Wang, *Nat. Commun.* **2015**, *6*, 7315.
[16] L. Li, F. Yang, G. J. Ye, Z. Zhang, Z. Zhu, W. Lou, X. Zhou, L. Li, K. Watanabe, T. Taniguchi, K. Chang, Y. Wang, X. H. Chen, Y. Zhang, *Nat. Nanotechnol.* **2016**, *11*, 593.
[17] G. Long, D. Maryenko, J. Shen, S. Xu, J. Hou, Z. Wu, W. K. Wong, T. Han, J. Lin, Y. Cai, R. Lortz, N. Wang, *Nano Lett.* **2016**, *16*, 7768.
[18] C. Husko, J. Kang, G. Moille, J. D. Wood, Z. Han, D. Gosztola, X. Ma, S. Combrié, A. De Rossi, M. C. Hersam, X. Checoury, J. R. Guest, *Nano Lett.* **2018**, *18*, 6515.
[19] J. Yang, R. Xu, J. Pei, Y. W. Myint, F. Wang, Z. Wang, S. Zhang, Z. Yu, Y. Lu, *Light: Sci. Appl.* **2015**, *4*, e312.
[20] C. Chen, F. Chen, X. Chen, B. Deng, B. Eng, D. Jung, Q. Guo, S. Yuan, K. Watanabe, T. Taniguchi, M. Lee, F. Xia, *Nano Lett.* **2019**, *19*, 1488.
[21] Y. Huang, J. Ning, H. Chen, Y. Xu, X. Wang, X. Ge, C. Jiang, X. Zhang, J. Zhang, Y. Peng, Z. Huang, Y. Ning, K. Zhang, Z. Zhang, *ACS Photonics.* **2019**, *6*, 1581.
[22] A. Surrente, A. A. Mitioglu, K. Galkowski, W. Tabis, D. K. Maude, P. Plochocka, *Phys. Rev. B* **2016**, *93*, 121405.
[23] C. E. P. Villegas, A. R. Rocha, A. Marini, *Nano Lett.* **2016**, *16*, 5095.
[24] B. Mamoru, N. Yoshitaka, S. Kiyotaka, M. Akira, *Jpn. J. Appl. Phys.* **1991**, *30*, L1178.
[25] M. Leroux, N. Grandjean, B. Beaumont, G. Nataf, F. Semond, J. Massies, P. Gibart, *J. Appl. Phys.* **1999**, *86*, 3721.
[26] O. Salehzadeh, M. Djavid, N. H. Tran, I. Shih, Z. Mi, *Nano Lett.* **2015**, *15*, 5302.
[27] T. Schwarzl, G. Springholz, M. Böberl, E. Kaufmann, J. Roither, W. Heiss, J. Fürst, H. Pascher, *Appl. Phys. Lett.* **2005**, *86*, 031102.
[28] X. Zhuang, P. Guo, Q. Zhang, H. Liu, D. Li, W. Hu, X. Zhu, H. Zhou, A. Pan, *Nano Res.* **2016**, *9*, 933.
[29] J. Shang, C. Cong, Z. Wang, N. Peimyoo, L. Wu, C. Zou, Y. Chen, X. Y. Chin, J. Wang, C. Soci, W. Huang, T. Yu, *Nat. Commun.* **2017**, *8*, 543.